Molecular mechanisms regulating the establishment of hepatocyte polarity during human hepatic progenitor cell differentiation into a functional hepatocyte-like phenotype

Mingxi Hua*, Weitao Zhang*, Weihong Li, Xueyang Li, Baoqing Liu, Xin Lu and Haiyan Zhang‡

Department of Cell Biology, Municipal Laboratory for Liver Protection and Regulation of Regeneration, Capital Medical University, Beijing, 100069, China

*These authors contributed equally to this work
‡Author for correspondence (culture@ccmu.edu.cn)

Accepted 6 August 2012
Journal of Cell Science 125, 5800–5810

doi: 10.1242/jcs.110551

Summary

The correct functioning of hepatocytes requires the establishment and maintenance of hepatocyte polarity. However, the mechanisms regulating the generation of hepatocyte polarity are not completely understood. The differentiation of human fetal hepatic progenitor cells (hFHPCs) into functional hepatocytes provides a powerful *in vitro* model system for studying the molecular mechanisms governing hepatocyte development. In this study, we used a two-stage differentiation protocol to generate functional polarized hepatocyte-like cells (HLCs) from hFHPCs. Global gene expression profiling was performed on triplicate samples of hFHPCs, immature-HLCs and mature-HLCs. When the differential gene expression was compared based on the differentiation stage, a number of genes were identified that might be essential for establishing and maintaining hepatocyte polarity. These genes include those that encode actin filament-binding protein, protein tyrosine kinase activity molecules, and components of signaling pathways, such as *PTK7*, *PARD3*, *PRKCI* and *CDC42*. Based on known and predicted protein-protein interactions, the candidate genes were assigned to networks and clustered into functional categories. The expression of several of these genes was confirmed using real-time RT-PCR. By inactivating genes using small interfering RNA, we demonstrated that *PTK7* and *PARD3* promote hepatic polarity formation and affect F-actin organization. These results provide unique insight into the complex process of polarization during hepatocyte differentiation, indicating key genes and signaling molecules governing hepatocyte differentiation.

Key words: Hepatic progenitor cells, Differentiation, Hepatocyte polarity, Gene expression

Introduction

As for all epithelial cells, hepatocytes must be polarized to be functional in the adult liver. That is, the correct function of the liver is ensured by the establishment and maintenance of hepatocyte polarity. The polarization of hepatocytes involves the formation of functionally distinct apical and basolateral plasma membrane domains. The apical poles of front-facing and adjacent hepatocytes form a continuous network of bile canaliculi (BC), which is in contact with the external environment, into which bile is secreted. The basal membrane domain (sinusoidal), which is in contact with the blood, secretes various components into the circulation and is responsible for the uptake of recycled biliary salts. In polarized hepatocytes, the tight junctions (TJs) create the border between apical and lateral poles (Wang and Boyer, 2004; Decaens et al., 2008). Perturbation or loss of polarity is a hallmark of many hepatic diseases, e.g. cholestasis. A complete understanding of the molecular mechanisms involved in hepatocyte polarization is therefore of considerable significance to both liver cell biology and the pathogenesis of liver diseases. However, hepatocyte polarization is still poorly understood.

The establishment of hepatocyte polarity begins during liver embryogenesis. During hepatocyte differentiation, specific routes and mechanisms are defined for the delivery of proteins to the plasma membrane (Wang and Boyer, 2004; Lemaigre and Zaret, 2004; Lemaigre, 2009). Using microarray analysis, several studies have examined the key genes and pathways of potential importance for generating hepatocyte-like cells (HLCs). In these reports, the liver-specific gene expression was identified within the total, heterogeneous population of cells that differentiated from human embryonic stem cells (Chiao et al., 2008; Synnergren et al., 2010; Jozefczuk et al., 2011) and induced pluripotent stem cells (Jozefczuk et al., 2011), HepaRG liver progenitor cells (Parent and Beretta, 2008) or human adipose tissue-derived stromal cells (Bonora-Centelles et al., 2009; Saulnier et al., 2010). Although these systems have limitations inherent to their respective origins, they represent human models of hepatocyte differentiation. To gain the most specific insight possible into the molecular events driving the establishment of hepatocyte polarity, analyses should be performed on purified cells with specific lineage markers. Human fetal hepatic progenitor cells (hFHPCs) were isolated based on alpha-fetoprotein (AFP) promoter expression from fetus that were aborted during the first trimester (Wang et al., 2008). They express AFP, albumin (ALB), cytokeratin 19 (CK19), are able to

Journal of Cell Science

proliferate long-term *in vitro* (Wang et al., 2008) and can differentiate into functional HLCs *in vitro* (Zhang et al., 2012). Thus, hFHPCs are a potential source and a useful model system to study the mechanisms that regulate the process of hepatocyte differentiation.

In this study, we used a two-stage differentiation protocol to generate functional and polarized HLCs from hFHPCs and performed global gene expression profiling on undifferentiated hFHPCs, immature-HLCs, and mature-HLCs. By comparing differential gene expression profiles of different stages of differentiation, a common pool of genes that serve as regulators of hFHPCs differentiation were identified. Subsequently, the genes involved in cell morphogenesis were further investigated for their molecular functions and their roles in the interactive network of genes associated with hepatocyte polarity. We identified *PTK7*, *PARD3*, *PRKCI* and *CDC42*, known to play key roles in the establishment or maintenance of cell polarity, as genes that were regulated during hFHPCs differentiation. CDC42 may be a core factor in regulating hepatocyte polarization. The expression of several of these genes was confirmed using real-time RT-PCR. The function of two genes (*PTK7* and *PARD3*) in the formation of hepatic polarity was further explored by inactivating their expression using small interfering RNA (siRNA) technology.

Results

Differentiation of hFHPCs into functional hepatocyte-like cells

We previously established a protocol to isolate fetal hepatic progenitor cells based on AFP promoter expression from human aborted fetus, and produced hFHPCs using this protocol (Wang et al., 2008). hFHPCs express the hepatic stem cells/progenitor cells marker AFP, ALB, CK19, epithelial cell adhesion molecule (EpCAM) (Schmelzer et al., 2006; Inada et al., 2008), Delta-like protein (Dlk) (Yanai et al., 2010), and sal-like protein 4 (Sall4) (Oikawa et al., 2009) (supplementary material Fig. S1A). In this study, we used a two-stage differentiation protocol to differentiate of hFHPCs into functional HLCs. In the first stage, hFHPCs were induced to become immature hepatic cells by 5 days of HGF treatment. In the second stage, the immature hepatic cells were further matured by the combination of HGF, DEX and OSM treatment for another 5 days. The majority of the differentiated cells at day 5 showed an epithelial morphology with binucleated centers, expressed lower levels of AFP, and expressed higher levels of ALB and CK8 than at day 0. The differentiated cells at day 10 exhibited typical hepatocyte morphology with a polygonal shape, containing distinctly round nuclei with one or two prominent nucleoli and intercellular structures resembling hepatic canaliculi. They did not express AFP, but the levels of ALB and CK8 significantly increased over day 5 (Fig. 1A; supplementary material Fig. S1B).

To further characterize the cells, glycogen storage, ALB secretion and CYP450 enzyme activity were detected in cells at different time points. As shown in Fig. 1B, nearly all the cells at day 10 stained positive for periodic acid-Schiff (PAS), whereas no positive staining was visible in the progenitor cells and the HGF-induced cells. Similar to PAS staining, the ALB secretion rate from cells at day 5 and day 10 were significantly upregulated compared to that at day 0 (Fig. 1C). As expected, ~90±2.5% of the differentiated cells at day 10 exhibited CYP2B1/2 activity, compared to 10±4.3% of the cells at day 5 (Fig. 1D). The CYP1A1 and CYP1A2 activities in the cells at day 10 were greater than the equivalent activities in the cells at day 5 (Fig. 1E). These results suggest that this differentiation protocol gives rise to functional HLCs.

Differentiation of hFHPCs into polarized hepatocyte-like cells

In parallel to functional differentiation, hFHPCs undergo cell morphogenesis and may acquire polarity. To determine whether hepatocyte polarity is established in this differentiation process, the assembly of TJs was analyzed at different time points. The localization of TJ-associated protein ZO-1 and F-actin were

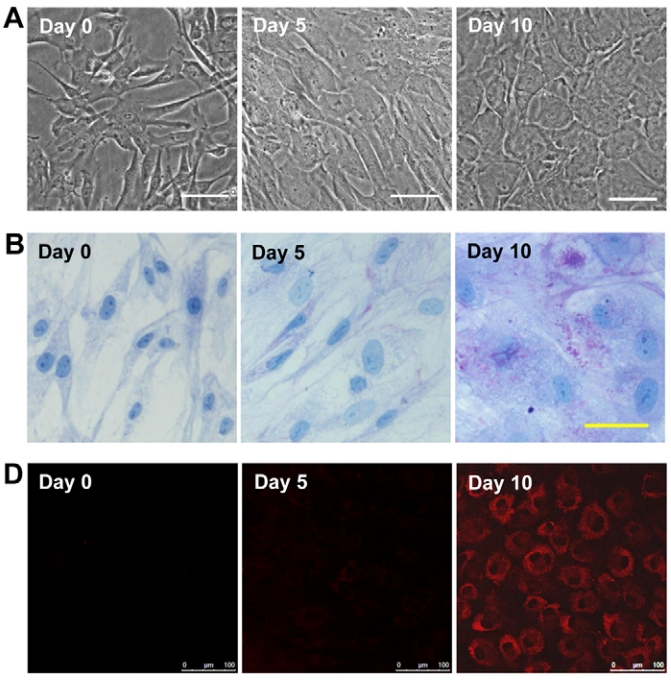

Fig. 1. Functional properties of hFHPCs and their progeny. (**A**) Morphology of cells under phase-contrast microscopy at different time points. (**B**) Intracellular glycogen in the hFHPCs was analyzed by PAS staining at different time points. (**C**) Albumin secretion was analyzed by ELISA. **P*<0.05 compared with day 0. (**D**) CYP2B1/2 enzyme activity in the differentiated hFHPCs was evaluated by PROD assay at different time points. (**E**) Activity of CYP1A1 and CYP1A2 was measured by EROD and MROD, respectively. **P*<0.05 compared with day 5. The data are presented as the mean ± s.d. (*n*=3). Scale bars: 50 μm unless labeled otherwise.

detected using anti-ZO-1 and FITC-conjugated phalloidin and visualized with confocal microscopy. As shown in Fig. 2A, we examined sections from day 0, day 5 and day 10 cultures in both the *x-z* and *x-y* planes. In *x-y* confocal images of hFHPCs (day 0), F-actin drew a network through the cells. In *x-z* cross-sections through the cells, small spots of ZO-1 were observed along an individual cell-cell border (Fig. 2A, left panel, arrow). After HGF stimulation for five days, F-actin was strongly concentrated at cell-cell boundaries, and in *x-z* confocal images, ZO-1 appeared as punctate spots at sites of cell-cell contact throughout the cell layer (Fig. 2A, middle panel, arrow). At day 10, thick F-actin bundles around the cells were increased in abundance and size; ZO-1 protein was concentrated along cell-cell borders in a linear pattern. At the same time, in *x-z* confocal images, ZO-1/F-actin double-staining spots increased at sites of cell-cell contact (Fig. 2A, right panel, arrow). The localization of another TJ-associated protein, junctional adhesion molecule A (JAM-A) (Braiterman et al., 2007; Paris et al., 2008), was determined later. Fig. 2B shows that JAM-A was predominantly expressed at the border of two adjacent cells at day 10. Moreover, ultra-thin sections displayed the TJ belt in hFHPC-derived HLCs (Fig. 2C). These results raise the possibility that TJs form between the hFHPC-derived HLCs during differentiation.

To test whether these morphogenetic features represent the acquisition of functional TJs, we evaluated the barrier function of TJs, the transepithelial electrical resistance (TER) and the paracellular fluxes. The values of TER in cells at day 5 and day 10 were significantly increased compared to the undifferentiated cells (day 0) (Fig. 2D). To determine the dynamic function of TJs, apical-to-basolateral FITC-dextran leakage across cultures was examined upon differentiation. In contrast to TER, which is an instantaneous measure of TJ functional integrity, FITC-dextran diffusion is measured over a period of 30 min and therefore may be a more sensitive measure of apical-to-basolateral leakage. The results reveal that permeability declined from day 6 after onward. Paracellular flux rates of FITC-dextran in differentiated cells at day 5, day 6, and day 8 were 101%, 81% and 69%, respectively, relative to that of the cells at day 0 (Fig. 2E).

To examine whether the hFHPC-derived HLCs formed BC-like structures, their ultra-structures were studied in cultures at day 10. Ultrathin sections displayed BC with microvilli (Fig. 3A, arrow) among the hFHPC-derived HLCs. To evaluate the functional activity of drug transporters in HLCs, 5(6)-carboxy-2,7-dichlorofluorescein diacetate (CDFDA) was added into the cultures at day 10 in the absence or presence of probenecid, an inhibitor of the multidrug resistance-associated protein (MRP) 2-mediated transport of 5 (and 6)-carboxy-2,7-dichlorofluorescein (CDF) in hepatocytes (Zamek-Gliszczynski et al., 2003). Fig. 3B shows that the fluorescent CDF was presented in the BC lumen among hFHPC-derived HLCs in the absence of probenecid. A significant decrease in CDF was observed in the BC lumen in the

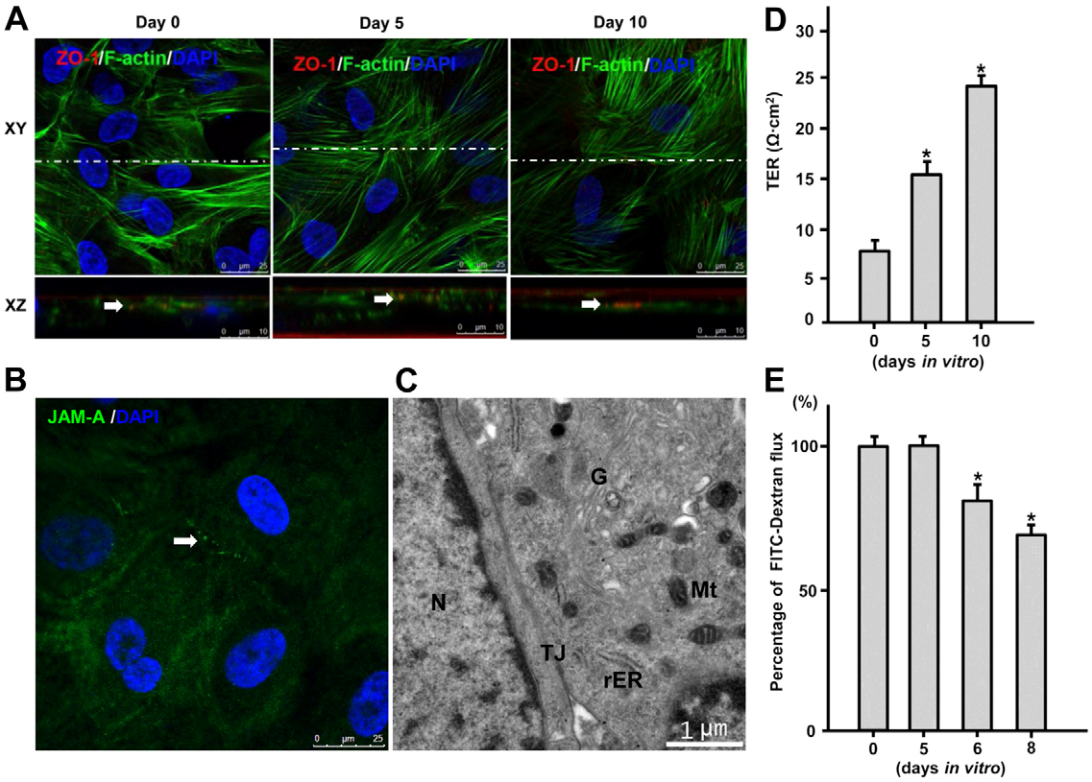

Fig. 2. TJ-associated structures and functions in hFHPCs and their progeny. (**A**) Cultured cells double-stained for ZO-1 and F-actin were imaged in the *x-y* plane and the *x-z* plane. The *x-z* planes taken as indicated (white line) on the corresponding *x-y* planes are shown. Arrows indicate the colocalization of ZO-1 and F-actin. (**B**) Cells at day 10 stained for JAM-A were imaged by confocal microscopy. Arrow indicates the localization of JAM-A. (**C**) Ultrathin section showing a TJ between the cells at day 10. N, nucleus; TJ, tight junction; rER, rough endoplasmic reticulum; G, Golgi; Mt, mitochondria. (**D**) Barrier function measured as TER in the differentiated hFHPCs at the indicated times. **P*<0.05 compared with day 0. (**E**). Barrier function measured as paracellular fluxes using FITC-dextran in the hFHPCs. **P*<0.05 compared with day 0. The data are presented as the mean ± s.d. (*n*=3).

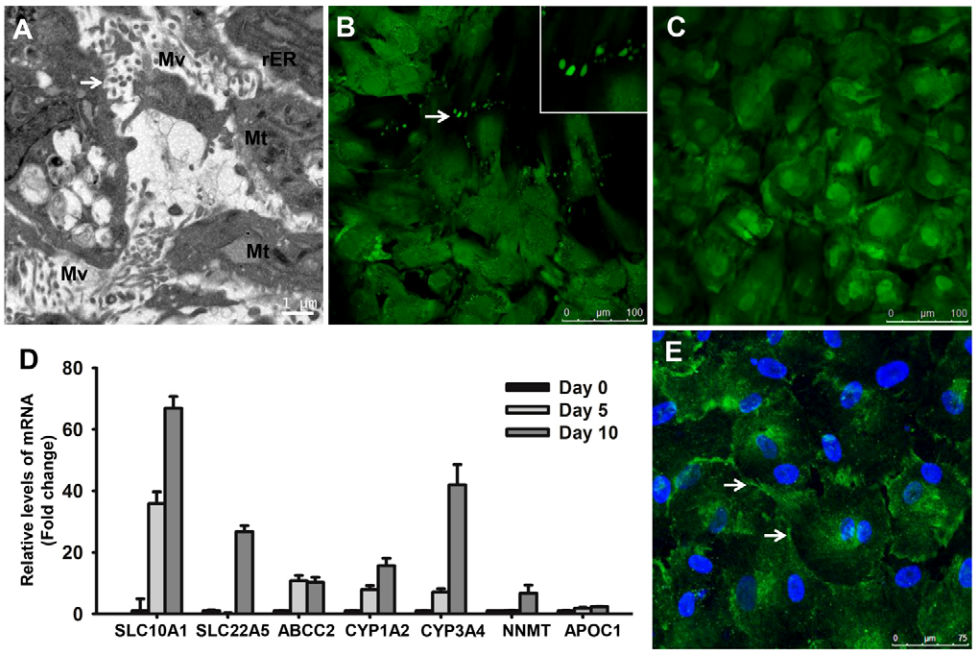

Fig. 3. Gene expression and functional polarization in hFHPC-derived HLCs. (**A**) Ultrathin section showing a BC among the cells. Arrows indicate the microvillus. Mv, microvillus; rER, rough endoplasmic reticulum; Mt, mitochondria. CDFDA is internalised by hFHPC-derived functional HLCs, cleaved by intracellular esterases and excreted into BC as fluorescent CDF without (**B**) and with (**C**) 4 mM probenecid. Arrows indicate the fluorescent CDF transported into BC. (**D**) Quantitative comparison of the transcription of phase I and phase II enzymes as well as drug transporters in hFHPCs and their progenies. SLC10A1, solute carrier family 10 (sodium/bile acid co-transporter family), member 1; SLC22A5, solute carrier family 22 (organic cation/carnitine transporter), member 5; ABCC2, ATP-binding cassette, sub-family C (CFTR/MRP), member 2; CYP1A2, cytochrome P450 1A2; CYP3A4, cytochrome P450 3A4; NNMT, nicotinamide *N*-methyltransferase; APOC1, apolipoprotein C-I. (**E**) hFHPC-derived HLCs stained for OATP were imaged by confocal microscopy. Arrows indicate OATP-positive staining.

presence of probenecid, suggesting that the excretion of CDF in hFHPC-derived HLCs was mediated by MRP2, a transporter in the apical pore of hepatocytes that functions canalicular secretion (Fig. 3C). Quantitative comparisons of gene expression reveal that the mRNA level of phase I/II enzymes as well as that of drug transporters in hFHPC-derived HLCs were significantly higher than in hFHPCs (Fig. 3D). Fig. 3E demonstrates the basal surface staining of the organic anion transporting polypeptide (OATP) (König et al., 2000) in hFHPC-derived HLCs. These results suggest that this differentiation protocol gives rise to functional polarized HLCs in a way that resembles natural hepatocyte development.

Differential gene expression and functional annotation analysis during hFHPC differentiation

To obtain an initial perspective on global gene expression changes, we performed a pairwise comparison of gene expression microarray data based on the stage of hFHPCs differentiation. A Volcano Plot filtering identified two major transitions in the gene expression patterns (supplementary material Fig. S2): undifferentiated hFHPCs to immature HLCs (stage I) and immature HLCs to mature HLCs (stage II). The microarray revealed that 1780 genes were significantly affected (814 upregulated and 966 downregulated) in stage I; 1835 genes were significantly affected (970 upregulated and 865 downregulated) in stage II. The regulated genes among the lists derived from the two stages were compared by a Venn diagram, which led to the classification of three gene sets: 514 significantly regulated genes were shared by the two stages; 1266 genes were unique to stage I; 1321 regulated genes were unique to stage II (supplementary material Fig. S3A). The 514 overlapping genes were classified into four gene subsets by the hierarchical clustering (supplementary material Fig. S3B; Table S2).

Functional gene annotation analysis of differentially expressed genes was performed according to the gene subsets to explore the functions of the regulated genes in hFHPCs differentiation. Analysis of the significantly upregulated genes found in stage I led to the identification of functional groups, such as ‘cell adhesion’, ‘extracellular matrix organization’, and ‘anatomical structure morphogenesis’ (Fig. 4A; supplementary material Table S3-1). The downregulated gene functional groups in stage I included ‘cell cycle’, ‘organelle organization’, and ‘cellular metabolic process’ (Fig. 4B; supplementary material Table S3-2). A similar analysis was performed for regulated genes found in stage II, and the upregulated gene functional groups included: ‘alcohol metabolic process’, ‘glycolysis’, and ‘cellular amino acid metabolic process’ (Fig. 4C; supplementary material Table S4-1). The functional classification of the downregulated included groups: ‘cell-cell signalling’, ‘anatomical structure morphogenesis’, and ‘cellular developmental process’ (Fig. 4D; supplementary material Table S4-2). The ten most significantly overrepresented annotations within the functional classification of the regulated genes shared by the two stages are listed in supplementary material Table S5.

Taken together, these results suggest that the gene expression patterns of undifferentiated hFHPCs, immature HLCs and mature HLCs are in keeping with the changes in cell phenotypes, and

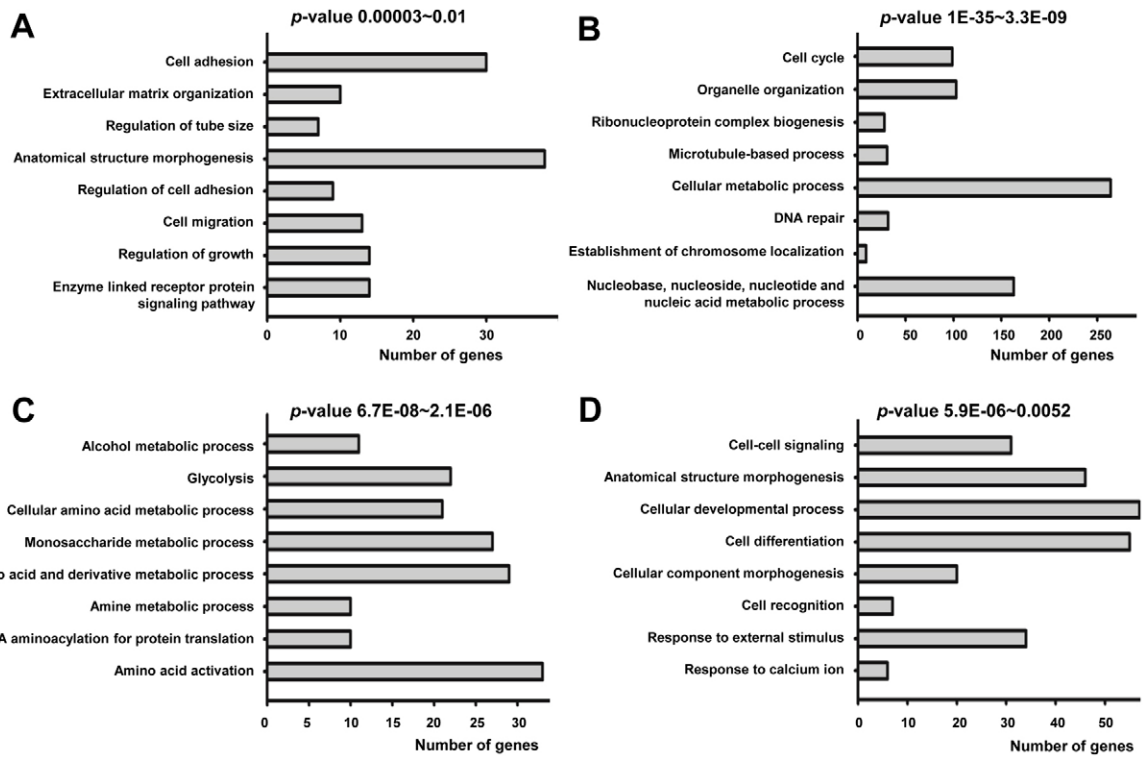

Fig. 4. Most enriched GO biological process terms for genes expressed differentially during hFHPC differentiation. (**A**) Most significant biological process (BP) terms for upregulated genes unique to stage I. (**B**) Most significant BP terms for downregulated genes unique to stage I. (**C**) Most significant BP terms for upregulated genes unique to stage II. (**D**) Most significant BP terms for downregulated genes unique to stage II.

reflecting the specific effects of regulators on hepatocyte differentiation.

Functional network analysis of the differentially expressed genes involved in cell morphogenesis

To gain a better understanding of the molecular mechanisms that regulate hepatocyte polarity generation during hFHPCs differentiation, the differentially expressed genes within the defined GO categories (GO 0000902: cell morphogenesis; GO 0022604: regulation of cell morphogenesis; GO 0010769: regulation of cell morphogenesis involved in differentiation) were selected for further examination. We found 63 genes (40 upregulated, 23 downregulated) in stage I and 69 genes (29 upregulated, 40 downregulated) in stage II, and 19 genes were common between the two stages (supplementary material Table S6). Among the common genes, six genes (*ADM*, *APOE*, *CDC42EP3*, *EFNB1*, *FBLIM1* and *THY1*) were upregulated, whereas *IL6*, *NOX4* and *RAC2* were downregulated, in both stages; eight genes (*ANTXR1*, *DFNB31*, *GDF7*, *ITGB4*, *LIMA1*, *MBP*, *MYH10* and *TGFB3*) were upregulated in stage I and downregulated in stage II. In contrast, *SPG3A* and *VEGF* were downregulated in stage I and upregulated in stage II (supplementary material Fig. S4).

Establishment of epithelial cell polarity is part of cell morphogenesis, which is driven by the forces that cells produce both internally and exert on neighboring cells. To examine the correlations between the candidate genes and hepatocyte polarization, the candidate genes were further categorized using GO analysis. The candidate genes were involved in 'establishment or maintenance of cell polarity', 'membrane organization', 'cell junction organization', and 'cytoskeleton organization' (Table 1). Interestingly, three gene subsets involved in the establishment or maintenance of cell polarity were identified. *PTK7*, *PARD3* and *PRKCI* were upregulated in stage I, with *PTK7* and *PRKCI* responsible for establishing or maintaining epithelial cell apical/basal polarity. *KNTC2*, *CDC42*, *CENPA* and *CCDC99* were downregulated in stage I, with *KNTC2*, *CENPA* and *CCDC99* responsible for establishing mitotic spindle orientation; *CAP2*, *DOCK2* and *NDE1* were downregulated in stage II, all of which are involved in cytoskeleton organization. One gene subset involved in membrane organization (*DAB2*, *APOE*, *MYH10*, *PRKCI* and *ULK1*) was upregulated in stage I, all of which are involved in 'vesicle-mediated transport'. Among the genes involved in cell junction organization, *THY1*, *GJA1*, *PRKCI* and *TGFB3* were upregulated in stage I; *SMAD3*, *SMAD7*, *CDC42* and *DLC1* were downregulated in stage I; and, *SHROOM2* and *TGFB3* were downregulated in stage II. *CDC42* and *PRKCI* are involved in the formation of epithelial TJs. Thus, the GO analysis showed that the candidate genes were assigned to the key biological processes required for cell polarization.

To better visualize the functional interactions at the network level, the candidate genes were submitted to functional network reconstruction using STRING. As shown in Fig. 5, 16 genes (*FYN*, *RHOJ*, *PLXNB1*, *DLC1*, *CDC42*, *NTN1*, *CDC42EP3*, *PARD3*, *EPHB3*, *EFNB1*, *PVRL1*, *PRKCI*, *TPM1*, *RAC2*, *LIMA1*, and *MYH10*) (Fig. 5A) were clustered together. Within this functional cluster, *CDC42*, *MYH10*, *PARD3* and *PRKCI* are involved in TJs, and *FYN*, *CDC42*, *PARD3* and *PVRL1* are involved in adherens junctions. *CLASP1*, *KNTC2* (*NDC80*), *CENPA*, *CCDC99* and *NDE1* participate in maintenance of

Table 1. Selected differential express genes involved in the HLCs polarity formation

Upregulated genes in Stage I
1. Establishment or maintenance of cell polarity (including apical/basal cell polarity): *PTK7*, *PARD3* and *PRKCI*
2. Regulation of cell shape: *CDC42EP3*, *FYN*, *FBLIM1*, *MYH10* and *RHOJ*
3. Regulation of cell size: *APBB1*, *DAB2*, *TGFB3*, *TGFBR3* and *ULK1*
4. Regulation of cellular component size: *LIMA1*, *APBB1*, *DAB2*, *TGFB3*, *TGFBR3* and *ULK1*
5. Cell junction organization: *THY1*,*GJA1*, *PRKCI* and *TGFB3*
6. Membrane organization: *DAB2*, *APOE*, *MYH10*, *PRKCI* and *ULK1*
7. Cellular component organization: *SMO*, *SLITRK5*, *SEMA5A*, *S100A4*, *RXRA*, *ROBO3*, *LAMB1*, *ITGA1*, *GDF7*, *EFNB1*, *DFNB31* and *ADM*
8. Regulation cellular component organization: *RUFY3*, *MBP*, *PLXNB2* and *PLXNB1*
9. Cellular component assembly: *BBS1*, *LIMA1*, *THY1*, *GJA1*, *APOE*, *ITGB4*, *MYH10*, *OFD1*, *PARD3* and *TTLL3*
10. Cytoskeleton organization: *BBS1*, *LIMA1*, *THY1*, *ANTXR1*, *DMD*, *APOE*, *MYH10*, *OFD1*, *PRKCI*, *RHOJ* and *TTLL3*
11. Actin cytoskeleton organization: *LIMA1*, *ANTXR1*, *MYH10*, *PRKCI*, *RHOJ* and *TTLL3*

Downregulated genes in Stage I
1. Establishment or maintenance of cell polarity: *KNTC2*, *CDC42*, *CENPA* and *CCDC99*
2. Regulation of cell shape: *DLC1* and *VEGF*
3. Cell junction organization: *SMAD3*, *SMAD7*, *CDC42* and *DLC1*
4. Cellular component organization: *TTL*, *CDC42*, *CCDC99*, *KNTC2*, *DLC1*, *SMAD7*, *SMAD3*, *RAC2*, *CENPA*, *VEGF*, *UCHL1*, *TRAPPC4*, *SPG3A*, *SH2B*, *NOX4*, *KIAA1893*, *IL6*, *HPRT1*, *HES1*, *GLI2*, *EGR2* and *CDH4*
5. Cytoskeleton organization: *KNTC2*, *CDC42*, *CENPA*, *CCDC99*, *DLC1*, *RAC2* and *TTL*
6. Actin cytoskeleton organization: *CDC42*, *DLC1* and *RAC2*
7. Regulation of actin filament bundle formation: *SMAD3* and *DLC1*

Upregulated genes in Stage II
1. Establishment or maintenance of cell polarity: *CLASP1*
2. Regulation of cell shape: *PALM2-AKAP2*, *CDC42EP3*, *FBLIM1* and *VEGF*
3. Cellular component organization: *ARL6*, *BCL6*, *DKFZP586P0123*, *JAK2*, *KLF7*, *L1CAM*, *THY1*, *ADM*, *SPG3A*, *COL4A3BP*, *CLASP1*, *EFNB1*, *APOE*, *HIF1A*, *IL7R*, *KIF3A*, *NFATC1*, *NUMBL*, *STK4*, *SLC1A3*, *STXBP1*, *UNC5B* and *CSPG2*
4. Regulation of cellular component organization: *PALM2-AKAP2*, *CDC42EP3*, *THY1*, *CLASP1*, *FBLIM1*, *APOE*, *LRRC4C*, *NUMBL*, *STXBP1* and *VEGF*
5. Cytoskeleton organization: *BCL6*, *THY1*, *CLASP1* and *APOE*

Downregulated genes in Stage II
1. Establishment or maintenance of cell polarity: *CAP2*, *DOCK2* and *NDE1*
2. Regulation of cell size: *NGFB*, *NTN1*, *PDGFB*, *SEMA3A* and *TGFB3*
3. Cell-cell junction organization: *SHROOM2* and *TGFB3*
4. Cellular component organization: *EPHB3*, *GDF7*, *CABP4*, *WNT3A*, *COL18A1*, *NOX4*, *SPON2*, *NRP2*, *PVRL1*, *PTPRF*, *GAP43*, *ETV4*, *BDNF*, *IL6*, *EGFR*, *CHRNB2* and *DFNB31*
5. Regulation of cellular component organization: *CHRNB2*, *MBP*, *PVRL1*, *PTPRF* and *TTC3*
6. Cellular component assembly: *FGD6*, *LIMA1*, *GAS7*, *ITGB4*, *MYH10*, *NRXN3*, *ONECUT2*, *PDGFB*, *RAC2*, *TPM1* and *VANGL2*
7. Regulation of cellular component size: *LIMA1*, *NGFB*, *NTN1*, *PDGFB*, *SEMA3A*, *SHROOM2* and *TGFB3*
8. Cytoskeleton organization: *CAP2*, *FGD6*, *LIMA1*, *ANTXR1*, *DOCK2*, *GAS7*, *MYH10*, *NDE1*, *PDGFB*, *RAC2* and *TPM1*
9. Actin cytoskeleton organization: *FGD6*, *LIMA1*, *ANTXR1*, *DOCK2*, *GAS7*, *MYH10*, *PDGFB*, *RAC2* and *TPM1*
10. Actin filament bundle formation: *LIMA1* and *GAS7*
11. Regulation of actin cytoskeleton organization: *LIMA1*, *SHROOM2* and *TPM1*

kinetochore integrity and kinetochore-microtubule attachments (Fig. 5B).

Confirmation of the differential expression of genes by real-time RT-PCR

To validate the accuracy of the gene indexes calculated from the microarray, six differentially expressed genes selected based on their roles in hepatocyte function (*ABCA1*, *CPS1* and *PCK2*) or cell morphogenesis (*APOE*, *CDC42* and *PTK7*) were confirmed by real-time RT-PCR. Comparison of the microarray and real-time RT-PCR results with their correlation coefficients are presented in Fig. 6. The data reveal that our gene index calculations from the microarray data accurately represented the expression of genes across a wide range of expression levels.

Functional analysis of candidate genes involved in the hepatocyte polarity

As a proof of principle, *PTK7* and *PARD3* were selected from the differentially expressed genes involved in hepatocyte polarity based on their unique cellular function. By reducing their expression level using siRNA, their effects on the formation of hepatocyte polarity during hFHPC differentiation were assessed. As shown in Fig. 7A, we successfully reduced the *PTK7* and *PARD3* expression level by 80–90% compared to the transfection control. The reduction of *PTK7* and *PARD3* significantly decreased the TER and increased the paracellular fluxes over a period of 30–120 min at 6 days post-transfection (Fig. 7B,C).

To identify morphology changes, hFHPCs with reduced expression of *PTK7* and *PARD3* were challenged to undergo differentiation into hepatocytes using our two-stage differentiation protocol. As shown in Fig. 7D, cells with inactivated *PTK7* and *PARD3* were unable to acquire the typical epithelial morphology, which exhibited the effects on F-actin assembly and apical actin concentration. Furthermore, the Golgi apparatus was randomly distributed in the cytoplasm in *PTK7* and *PARD3* knockdown cells, while the Golgi apparatus was localized between the nucleus and apical pole in control cells. These data demonstrate that reduction of either *PTK7* or *PARD3* may inhibit hepatocyte polarity formation during hFHPC differentiation.

Discussion

Generation of membrane polarity in hepatocytes is key developmental program and a multistage process that requires cell-cell interactions and the specific organization of proteins and lipids on the cell surface and in cell interior, which leads to modeling the complex architecture during hepatocyte

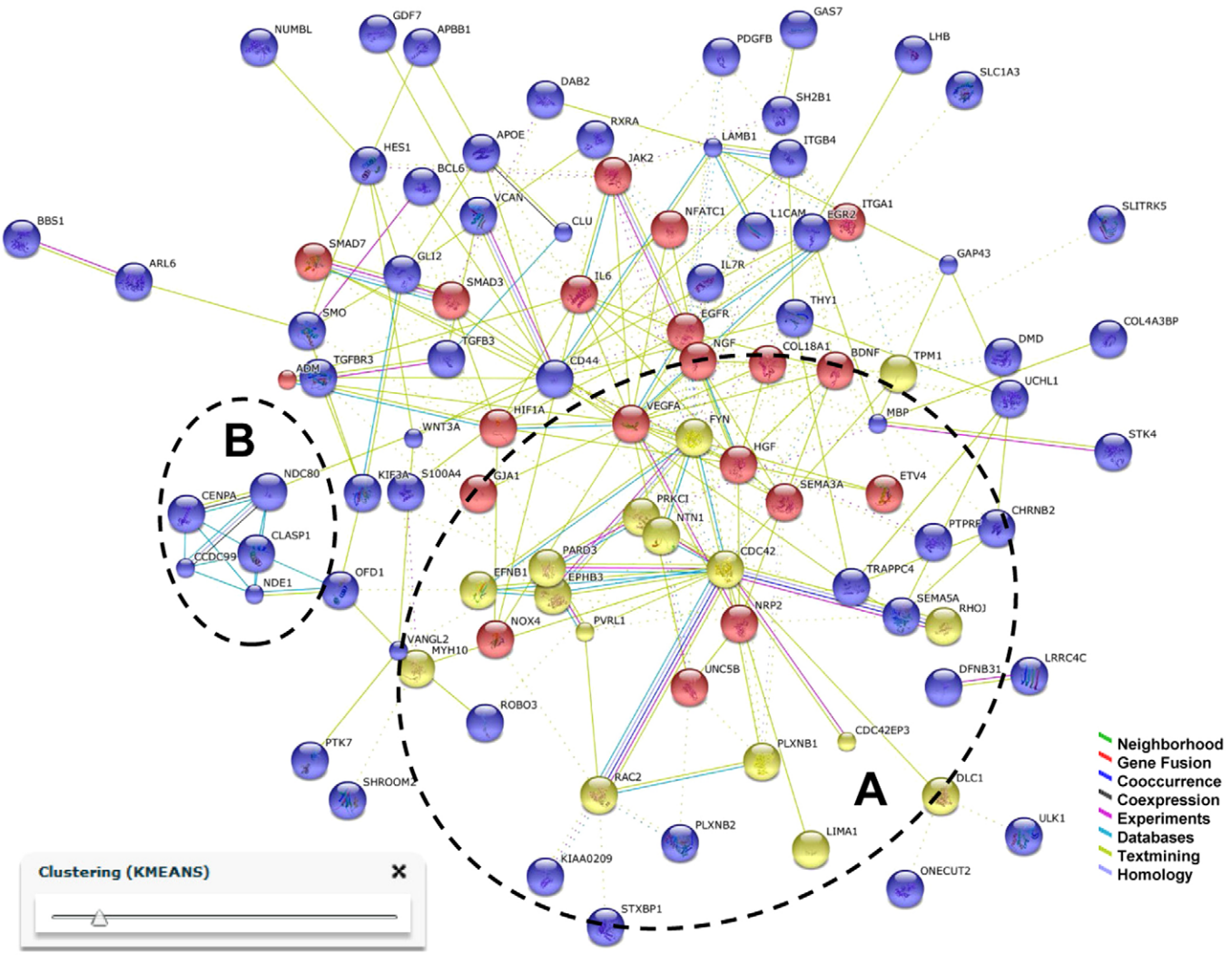

Fig. 5. Predicted protein network visualization with STRING. The network view predicted the associations between proteins from the regulated genes involved in cell morphogenesis during hFHPC differentiation. The network nodes are proteins. The edges represent the predicted functional associations with seven differently colored lines. These proteins were clustered using KMEANS clustering algorithms, depicted in the panel (arrow). Every color of node corresponds to a cluster. A and B indicate the identified clusters.

differentiation (Wang and Boyer, 2004; Takashi et al., 2007). Although information has recently been accumulated suggesting specific routes and mechanisms for this process (Matsui et al., 2002; Michalopoulos et al., 2003; Imamura et al., 2007; Chiao et al., 2008; Bonora-Centelles et al., 2009; Kidambi et al., 2009; Saulnier et al., 2010; Synnergren et al., 2010; Jozefczuk et al., 2011; Fu et al., 2011), the exact mechanism for hepatocyte polarity generation is unclear partly because only a few *in vitro* models are available for developing complex human hepatocyte polarity (Decaens et al., 2008). The goal of this study was to generate functional polarized hepatocytes from the hFHPCs *in vitro* and to explore the molecular mechanisms involved in hepatocyte polarization.

First, we found that sequential treatment of hFHPCs with HGF, OSM, and DEX is efficient to generate functional hepatocyte polarity in hFHPC-derived hepatocytes, which mimics hepatocyte differentiation both morphologically and functionally and resembles the natural hepatocyte development (Kinoshita et al., 1999; Kamiya et al., 2001; Zorn, 2008). We observed that hFHPCs were unpolarised with spindle-shaped morphology and possessed higher AFP and lower ALB expression under the initial culture conditions. After HGF treatment, the cells developed a simple polar phenotype with the establishment of functional TJs at the points of cell-cell contact along the cell perimeters, as evidenced by the zonular assembly of F-actin, ZO-1 and JAM-A through the function of TJs (TER and paracellular flux). These results suggest that HGF stimulates a morphogenesis of tight and functional integrity in the early stage of hFHPC differentiation, which is in line with previous reports (Pollack et al., 2004). In stage II, the immature cells were induced with HGF, OSM and DEX, and the multipolar hepatic phenotype gradually manifested itself during this period. Parallel to the observed morphological changes, ALB secretion, bile acid synthesis, glycogen storage and CYP450 enzyme activity accelerated, suggesting that the hepatocytes polarized rapidly. The formation of the BC architecture and the establishment of the hepatobiliary transport system in hFHPC-derived HLCs was further confirmed by electron microscopy and hepatocyte uptake assays. Taken together, our data suggest that a

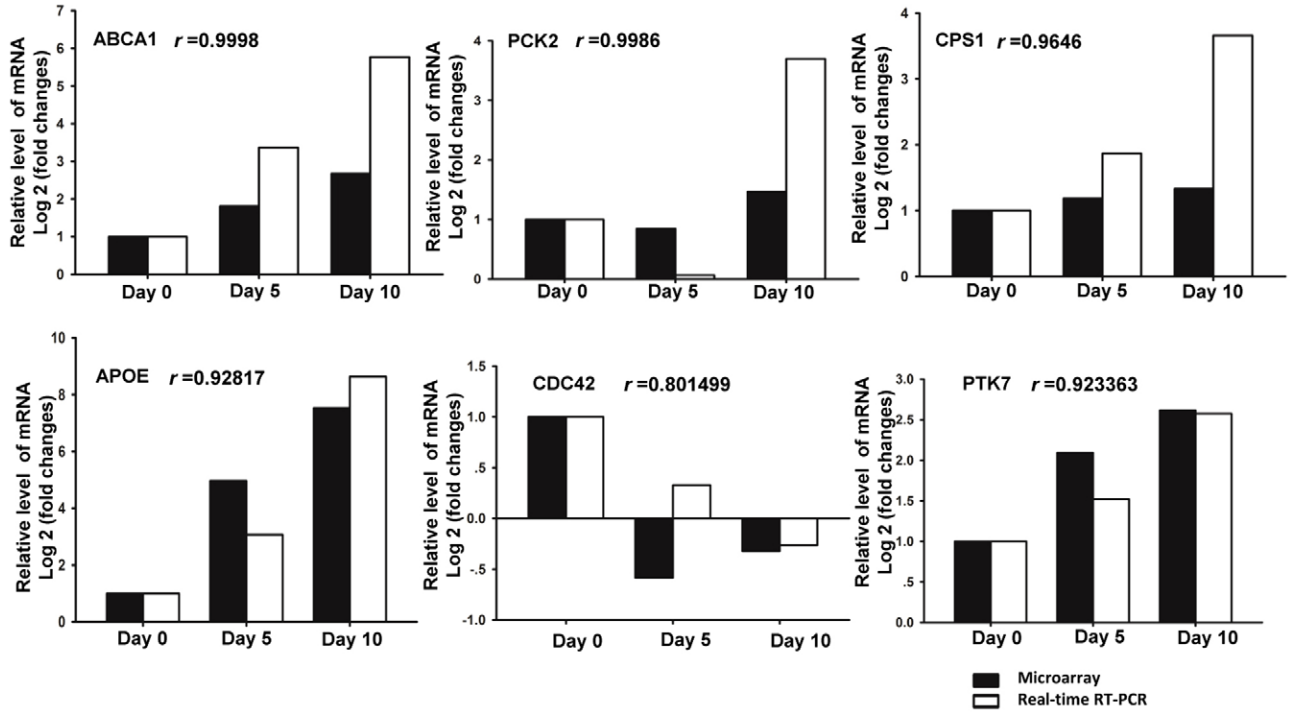

Fig. 6. Gene indexes from the microarray validated by real-time RT-PCR. The expression levels of six genes of interest in the hFHPCs were verified by real-time RT-PCR. The relative expression of each gene was normalized against 18S rRNA. Shown is a $\log_2$ plot of the fold changes, *r* indicates the correlation coefficients. ABCA1, ATP-binding cassette, sub-family A (ABC1), member 1; PCK2, phosphoenolpyruvate carboxykinase 2; CPS1, carbamoyl-phosphate synthase 1, mitochondrial; APOE, apolipoprotein E; CDC42, cell division cycle 42 (GTP binding protein); PTK7, PTK7 protein tyrosine kinase 7.

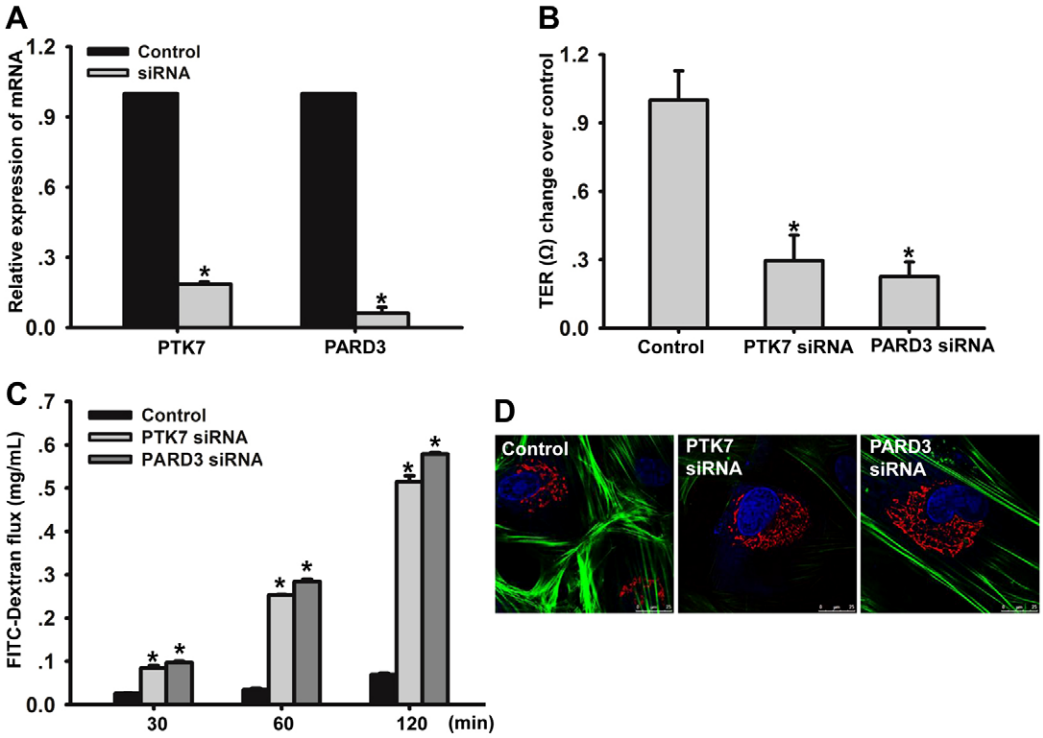

Fig. 7. Effect of gene reduction by siRNA transfection on hepatocyte polarity during hFHPC differentiation. (**A**) Real-time RT-PCR analysis of the transcript levels of the *PTK7* and *PARD3* genes 24 hours after siRNA transfection. Non-targeting siRNAs were used as a control. (**B**) Barrier function was measured as TER 24 hours after siRNA transfection in hFHPCs cultured in the presence of induction medium with HGF alone for 5 days. (**C**) Barrier function was measured as paracellular fluxes using FITC-dextran 24 hours post-siRNA transfection in hFHPCs cultured in the presence of induction medium with HGF alone for 5 days. (**D**) Localization of F-actin and Golgi 24 hours after siRNA transfection in hFHPCs cultured in the presence of induction medium with HGF for 5 days and HGF, OSM and DEX for another 5 days. Green, F-actin; red, Golgi. The data are presented as the mean ± s.d. ($n=3$); *$P<0.05$ compared with control.

human hepatocyte polarity was gradually generated during hFHPC differentiation *in vitro*. Therefore, this system may be a useful platform to explore the mechanisms of hepatocyte differentiation and hepatic polarity establishment.

Second, using high-density oligonucleotide microarrays, the global transcriptional profile of hFHPCs and their derivatives was investigated based on the stage of differentiation. We found 1780 genes in stage I and 1835 genes in stage II that were significantly regulated. From comparison of the transcriptional profiles between the two differentiation regimes, three main subsets of regulated genes were identified. Within each subset, the functional profiling of the upregulated and downregulated genes was further investigated using GO analysis. The upregulated genes in stage I were mainly involved in 'cell adhesion', 'extracellular matrix organization', and 'anatomical structure morphogenesis'. The upregulated genes in stage II were mainly involved in 'alcohol metabolic process', 'glycolysis', and 'cellular amino acid metabolic process'. Results revealed a dramatic switch in functional profile as proliferating hFHPCs differentiated into HLCs, which was in accordance with the cell phenotypes and previous reports on liver development (Lemaigre, 2009; Duncan, 2003; Zorn, 2008). These results present a detailed characterization of a unique set of genes, which can be used to explore the mechanisms of hepatocyte differentiation.

To examine which molecules govern hepatocyte morphogenesis, including polarization during differentiation, a subset of regulated genes (which included 113 genes) annotated as being associated with 'cell morphogenesis' in the two stages was selected (supplementary material Table S6) to explore the core regulated genes that are potentially involved in hepatocyte polarization. As expected, our data (Table 1) indicated that these core genes were involved in the key process of polarization, such as in apical/basal cell polarity and junction organization. Among them, *PTK7* (Lhoumeau et al., 2011; Puppo et al., 2011), *PARD3* (Ooshio et al., 2007; Achilleos et al., 2010; Ishiuchi and Takeichi, 2011), *PRKCI* (Eder et al., 2005), *CDC42* (Harris and Tepass, 2010), and *CLASP1* (Miller et al., 2009) have recently been identified to have roles in cell polarity. Our results demonstrated that *PTK7* and *PARD3* promote the formation of hepatic polarity and affect F-actin organization. The network analysis of the candidate genes, based on known and predicted protein-protein interactions, further illustrated the interactions of the molecules that regulate hepatocyte polarization and clustered them into functional categories. Sixteen genes (*FYN*, *RHOJ*, *PLXNB1*, *DLC1*, *CDC42*, *NTN1*, *CDC42EP3*, *PARD3*, *EPHB3*, *EFNB1*, *PVRL1*, *PRKCI*, *TPM1*, *RAC2*, *LIMA1* and *MYH10*) may be the functionally regulated modules for hepatocyte polarity generation.

In conclusion, our results provide insights into understanding hepatocytes polarization at the transcriptional level and reveal novel key genes and a functional network of potential importance for future efforts in exploring hepatic differentiation.

Materials and Methods

Culture and differentiation of hFHPCs

hFHPCs were prepared as described previously (Wang et al., 2008) with the informed patient consent and under the approval of the Ethics Committee of Capital Medical University (Beijing, China) for this project. hFHPCs were maintained in MEM/NEAA (Hyclone, Logan, UT) containing 5% fetal bovine serum (FBS, Hyclone), 100 U/mL penicillin, 100 μg/mL streptomycin, 20 ng/mL epidermal growth factor (EGF, Peprotech, Rocky Hill, NJ) and 10 μg/mL insulin (Sigma-Aldrich, St Louis, MO). Cells from passages nine to eleven were used in the study.

To induce of hepatocyte maturation, the cells were plated at 2×10^4 cells/cm^2 in culture plates and dishes, in expansion medium. Once cells reached 95% confluence, they were washed twice with PBS and differentiated in basal medium [MEM/NEAA, supplemented with 0.5 mg/mL albumin fraction V (Sigma-Aldrich), 100 U/mL penicillin, 100 μg/mL streptomycin, and 1% insulin-transferrin selenium (ITS, Sigma-Aldrich)] containing 20 ng/mL hepatocyte growth factor (HGF, Peprotech) for 5 days. Then, the differentiated cells were further matured in basal medium containing 20 ng/mL HGF, 10 ng/mL oncostatin M (OSM, Peprotech) and 10^{-7} M dexamethasone (DEX, Sigma-Aldrich) for another 5 days. Differentiation media were changed every 2 days.

Immunofluorescence staining

The cells were fixed with 4% paraformaldehyde for 20 min at room temperature, followed by permeabilize with 0.3% Triton X-100 in PBS for 5 min and then, rinsed and blocked with 20% goat serum (Zsgb-Bio, China) for 60 min at room temperature. The cells were then incubated with rabbit anti-ZO-1 at 1:200 (Invitrogen, Carlsbad, CA), mouse anti-JAM-A at 1:100 (F11R, BD Biosciences, San Jose, CA), or goat anti-OATP at 1:100 (Santa Cruz Biotechnology, Santa Cruz, CA); rabbit anti-AFP at 1:200 (Product Number A0008, Dako); mouse anti-ALB at 1:500 (clone HAS-11, Product Number A 6684, Sigma-Aldrich); mouse anti-CK8 at 1:200 (Product Number A, C5301, Sigma-Aldrich); mouse anti-EpCAM at 1:400 (Cell Signaling, MA); rabbit anti-Dlk at 1:500 (Abcam, Hong Kong) and rabbit anti-Sall4 at 1:50 (Abgent, San Diego, CA) at 4℃ overnight. Following three 5-min washes in PBS with gentle agitation, an Alexa Fluor-conjugated secondary antibody (1:500; Invitrogen) was added, and the samples were incubated for 60 min at 37℃. Afterwards, the cells were incubated with a mixture of FITC-labeled phalloidin (Sigma-Aldrich) and the nuclear stain DAPI (Sigma-Aldrich) at room temperature for 20 min. The cells were then washed and examined under a Leica TCS SP5 Confocal Microscope (Leica, Wetzlar, Germany). Photomultiplier settings were adjusted to the brightest signal and maintained during data acquisition. Samples were imaged either in the *x-y* plane or in the *x-z* plane.

Assay of Golgi apparatus localization

To mark the Golgi apparatus, a plasmid containing the sequence of the Golgi-resident enzyme N-acetylgalactosaminyltransferase 2 (GalNAc-T2) (Röttger et al., 1998) fused to red fluorescent protein (RFP) was transduced into cells using CellLight® Golgi-RFP *BacMam 2.0* (C10593, Invitrogen) (Kost et al., 2005) according to the manufacturers' instructions. Then, the labeled cells were fixed with 4% formaldehyde in PBS for 20 min at room temperature, followed by permeabilization with 0.3% Triton X-100 in PBS for 5 min at room temperature.

Transmission electron microscopy

For ultra-structural analysis, the differentiated cells were fixed in 2.5% glutaraldehyde in 0.1 M phosphate buffer, pH 7.2, for 60 min at 4℃. They were postfixed in 1% osmium tetroxide in 0.1 M phosphate buffer and embedded with the Spurr embedding kit. The sections were examined using an H-7650 electron microscope (Hitachi, Japan).

Glycogen assay

Intracellular glycogen was analyzed by PAS staining. Cultures were fixed in carnoy fixative at room temperature for 10 min and oxidised in 1% periodic acid for 15 min. After oxidation, the cultures were rinsed three times with distilled water and then treated with Schiff's reagent (Sigma-Aldrich) for 30 min. After the cells were rinsed with distilled water for 5 min, the cell nuclei were counterstained with Mayer's hematoxylin. The PAS-positive cells and whole cells were examined under a Leica light microscope (Leica).

Albumin analysis

The concentration of ALB secreted into the culture media was analyzed as previously described (Zhang et al., 2012).

Cytochrome P450 activity

To evaluate the activities of CYP1A1 and CYP1A2, ethoxyresorufin-O-deethylase (EROD) and methoxyresorufin-O-deethylase (MROD) assays were performed, respectively, as previously described (Donato et al., 1993; Kidambi et al., 2009). To evaluate the activity of CYP2B1/2, the penthoxyresorufin-O-deethylase (PROD) assay was performed. The differentiated cells were treated with 1 μM pentoxyresorufin and assessed under a Leica TCS SP5 Confocal Microscope (Leica). The PROD activity-positive cells were counted with Image-Pro Plus software (Media Cybernetics Inc., MD).

TER and permeability assay

To determine TER, cells were cultured to confluence in 12-mm Transwells with 0.4-μm pore size filters (Millipore, Billerica, MA). TER was measured in culture medium using a MILLICELL-ERS (Millipore) with 'chopstick' electrodes at different time points. For calculation, the resistance of blank filters was subtracted

from that of filters covered with cells to give the net resistance, which was multiplied by the membrane area to give the resistance in area-corrected units ($\Omega \cdot cm^2$). The data presented as the mean ± s.d.

To determine the paracellular flux, cells were cultured to confluence on 12-mm Transwells with 0.4-μm pore size filters (Millipore) and 2.5 mg/mL FITC-dextran (FD-70s, Sigma-Aldrich) was added to the inner chamber. The apparatus was then placed in a CO_2 incubator at 37℃ for 30, 60 and 120 min, respectively. Samples were collected from the outer chamber, and the fluorescent signals were measured at an excitation wavelength of 485 nm and emission wavelength of 535 nm using a spectrophotometer (Thermo Fisher Scientific Inc.). The results are expressed as the concentration of FITC-dextran in the outer chamber (mg/mL). The paracellular FITC-dextran flux rate was calculated as the measured value of the treated group relative to that of the control group.

At least three independent determinations of each parameter were compared among the treatment groups by one-way ANOVA using the statistical software SPSS 11.5. Differences were considered significant if $P<0.05$.

BC analysis

To determine the BC function, cells were incubated with 10 μM CDFDA (Sigma-Aldrich) in the absence or presence of 4 mM probenecid (Sigma-Aldrich) at 37℃ for 10 min to allow its internalization and subsequent translocation into the BC lumen by MRP 2 (Zamek-Gliszczynski et al., 2003; Turncliff et al., 2006). After extensive washes, the capacity of BC to contain the fluorescent CDF was analyzed under a Leica TCS SP5 Confocal Microscope (Leica).

Microarray experiments

Total RNA was isolated from undifferentiated hFHPCs and their derivatives in triplicate for each time point using TRIzol (Invitrogen) and the RNeasy kit (Qiagen, Hilden, Germany) according to the manufacturers' instructions, including a DNase digestion step. RNA quantity and purity were determined using the ND-1000 spectrophotometer (NanoDrop Technologies, Wilmington, DE) and denaturing gel electrophoresis. Approximately 5 μg total RNA of each sample was used for labeling with a NimbleGen one-color DNA labeling kit, array hybridization using the NimbleGen Hybridization System (NimbleGen 12×135K microarrays, Roche NimbleGen) and array scanning using the Axon GenePix 4000B microarray scanner (Molecular Devices Corporation, Sunnyvale, CA).

Data analysis

The raw data were extracted and normalized using NimbleScan v2.5 Software. The gene summary files were imported into Agilent GeneSpring Software (version 11.0) for further analysis. Genes that had values greater than or equal to the lower cutoff of 50.0 in all samples were chosen for further analysis. Genes that were differentially expressed with statistical significance were identified through Volcano Plot filtering (fold change ≥2.0 and P-value ≤0.05).

Similarities and differences among the differentially expressed genes at different stages were analyzed by Gene Venn (Hulsen et al., 2008). Differentially expressed genes in these lists were analyzed using the Database for Annotation, Visualization and Integrated Discovery (DAVID) tool (Huang et al., 2008) according to Gene Ontology (GO) roles. To examine potential interactions of genes involved in cell morphogenesis during the hFHPCs differentiation, we applied the Search Tool for the Retrieval of Interacting Genes (STRING) to predict the protein-protein interaction networks (Szklarczyk et al., 2011).

Real-time RT-PCR

Total cellular RNA was extracted from 1×10^6 cells with the RNeasy Mini Kit (QIAGEN) according to the manufacturer's instructions. For PCR analysis, 2 μg RNA was reverse-transcribed to cDNA using Superscript II reverse transcriptase and random hexamer primers (Invitrogen). Real-time PCR analysis was performed on an ABI Prism 7300 Sequence Detection System using the SYBR Green PCR Master Mix (Applied Biosystems, Foster City, CA). The reaction consisted of 10 μL of SYBR Green PCR Master Mix, 1 μL of a 5 μM mix of forward and reverse primers, 8 μL water, and 1 μL template cDNA in a total volume of 20 μL. Cycling was performed using the default conditions of the ABI 7300 SDS Software 1.3.1. The relative expression of each gene was normalized against 18S rRNA. The primers used are shown in supplementary material Table S1. The data are presented as the mean ± s.d.

siRNA Transfection

hFHPCs were plated at 2×10^4 cells/cm^2 in antibiotic-free basal medium 24 hours prior to transfection. siRNA transfection was performed following the manufacturer's protocol. Briefly, ON-TARGET SMARTpool siRNAs directed against *PTK7* (L-003167-00-0005, Dharmacon, Lafayette) or *PARD3* (L-015602-00-0005) or non-targeting siRNAs (D-001810-10-05) were mixed with Transfection DharmaFECT 4 (Dharmacon), respectively. After a 20-min incubation at room temperature, the complexes were added to the cells at a final siRNA concentration of 50 nM. The medium was replenished with medium containing antibiotic 24 hours post-transfection. Culture medium was then changed every 3 days for the duration of the experiment. hFHPCs transfected with non-targeting siRNAs were used as experimental control.

Statistics

Experiments were independently repeated three times with replicate samples. Statistical analysis was performed using one-way ANOVA tests using SPSS 11.5 statistics software. Differences were considered significant if $P<0.05$.

Acknowledgements

Microarray experiments were performed by KangChen Bio-tech, Shanghai, China.

Funding

This work was supported by grants from the National Natural Science Foundation of China [grant numbers 30971472, 31171310 to H. Z. and 81030009 to Liying Li]; and the Beijing Natural Science Foundation [grant number 5102013 to H. Z.].

Supplementary material available online at
http://jcs.biologists.org/lookup/suppl/doi:10.1242/jcs.110551/-/DC1

References

Achilleos, A., Wehman, A. M. and Nance, J. (2010). PAR-3 mediates the initial clustering and apical localization of junction and polarity proteins during *C. elegans* intestinal epithelial cell polarization. *Development* **137**, 1833-1842.

Bonora-Centelles, A., Jover, R., Mirabet, V., Lahoz, A., Carbonell, F., Castell, J. V. and Gómez-Lechón, M. J. (2009). Sequential hepatogenic transdifferentiation of adipose tissue-derived stem cells: relevance of different extracellular signaling molecules, transcription factors involved, and expression of new key marker genes. *Cell Transplant* **18**, 1319-1340.

Braiterman, L. T., Heffernan, S., Nyasae, L., Johns, D., See, A. P., Yutzy, R., McNickle, A., Herman, M., Sharma, A., Naik, U. P. et al. (2007). JAM-A is both essential and inhibitory to development of hepatic polarity in WIF-B cells. *Am. J. Physiol. Gastrointest. Liver. Physiol.* **294**, G576-G588.

Chiao, E., Elazar, M., Xing, Y., Xiong, A., Kmet, M., Millan, M. T., Glenn, J. S., Wong, W. H. and Baker, J. (2008). Isolation and transcriptional profiling of purified hepatic cells derived from human embryonic stem cells. *Stem Cells* **26**, 2032-2041.

Decaens, C., Durand, M., Grosse, B. and Cassio, D. (2008). Which *in vitro* models could be best used to study hepatocyte polarity? *Biol. Cell* **100**, 387-398.

Donato, M. T., Gómez-Lechón, M. J. and Castell, J. V. (1993). A microassay for measuring cytochrome P450IA1 and P450IIB1 activities in intact human and rat hepatocytes cultured on 96-well plates. *Anal. Biochem.* **213**, 29-33.

Duncan, S. A. (2003). Mechanisms controlling early development of the liver. *Mech. Dev.* **120**, 19-33.

Eder, A. M., Sui, X., Rosen, D. G., Nolden, L. K., Cheng, K. W., Lahad, J. P., Kango-Singh, M., Lu, K. H., Warneke, C. L., Atkinson, E. N. et al. (2005). Atypical PKCiota contributes to poor prognosis through loss of apical-basal polarity and cyclin E overexpression in ovarian cancer. *Proc. Natl. Acad. Sci. USA* **102**, 12519-12524.

Fu, D., Wakabayashi, Y., Lippincott-Schwartz, J. and Arias, I. M. (2011). Bile acid stimulates hepatocyte polarization through a cAMP-Epac-MEK-LKB1-AMPK pathway. *Proc. Natl. Acad. Sci. USA* **108**, 1403-1408.

Harris, K. P. and Tepass, U. (2010). Cdc42 and vesicle trafficking in polarized cells. *Traffic* **11**, 1272-1279.

Huang, da. W., Sherman, B. T. and Lempicki, R. A. (2008). Systematic and integrative analysis of large gene lists using DAVID bioinformatics resources. *Nat. Protoc.* **4**, 44-57.

Hulsen, T., de Vlieg, J. and Alkema, W. (2008). BioVenn – a web application for the comparison and visualization of biological lists using area-proportional Venn diagrams. *BMC Genomics* **9**, 488-494.

Imamura, M., Kojima, T., Lan, M., Son, S., Murata, M., Osanai, M., Chiba, H., Hirata, K. and Sawada, N. (2007). Oncostatin M induces upregulation of claudin-2 in rodent hepatocytes coinciding with changes in morphology and function of tight junctions. *Exp. Cell Res.* **313**, 1951-1962.

Inada, M., Follenzi, A., Cheng, K., Surana, M., Joseph, B., Benten, D., Bandi, S., Qian, H. and Gupta, S. (2008). Phenotype reversion in fetal human liver epithelial cells identifies the role of an intermediate meso-endodermal stage before hepatic maturation. *J. Cell Sci.* **121**, 1002-1013.

Ishiuchi, T. and Takeichi, M. (2011). Willin and Par3 cooperatively regulate epithelial apical constriction through aPKC-mediated ROCK phosphorylation. *Nat. Cell Biol.* **13**, 860-866.

Jozefczuk, J., Prigione, A., Chavez, L. and Adjaye, J. (2011). Comparative analysis of human embryonic stem cell and induced pluripotent stem cell-derived hepatocyte-like cells reveals current drawbacks and possible strategies for improved differentiation. *Stem Cells Dev.* **20**, 1259-1275.

Kamiya, A., Kinoshita, T. and Miyajima, A. (2001). Oncostatin M and hepatocyte growth factor induce hepatic maturation via distinct signaling pathways. *FEBS Lett.* **492**, 90-94.

Kidambi, S., Yarmush, R. S., Novik, E., Chao, P., Yarmush, M. L. and Nahmias, Y. (2009). Oxygen-mediated enhancement of primary hepatocyte metabolism, functional polarization, gene expression, and drug clearance. *Proc. Natl. Acad. Sci. USA* **106**, 15714-15719.

Kinoshita, T., Sekiguchi, T., Xu, M. J., Ito, Y., Kamiya, A., Tsuji, K., Nakahata, T. and Miyajima, A. (1999). Hepatic differentiation induced by oncostatin M attenuates fetal liver hematopoiesis. *Proc. Natl. Acad. Sci. USA* **96**, 7265-7270.

König, J., Cui, Y., Nies, A. T. and Keppler, D. (2000). Localization and genomic organization of a new hepatocellular organic anion transporting polypeptide. *J. Biol. Chem.* **275**, 23161-23168.

Kost, T. A., Condreay, J. P. and Jarvis, D. L. (2005). Baculovirus as versatile vectors for protein expression in insect and mammalian cells. *Nat. Biotechnol.* **23**, 567-575.

Lemaigre, F. P. (2009). Mechanisms of liver development: concepts for understanding liver disorders and design of novel therapies. *Gastroenterology* **137**, 62-79.

Lemaigre, F. and Zaret, K. S. (2004). Liver development update: new embryo models, cell lineage control, and morphogenesis. *Curr. Opin. Genet. Dev.* **14**, 582-590.

Lhoumeau, A. C., Puppo, F., Prébet, T., Kodjabachian, L. and Borg, J. P. (2011). PTK7: a cell polarity receptor with multiple facets. *Cell Cycle* **10**, 1233-1236.

Matsui, T., Kinoshita, T., Morikawa, Y., Tohya, K., Katsuki, M., Ito, Y., Kamiya, A. and Miyajima, A. (2002). K-Ras mediates cytokine-induced formation of E-cadherin-based adherens junctions during liver development. *EMBO J.* **21**, 1021-1030.

Michalopoulos, G. K., Bowen, W. C., Mulè, K. and Luo, J. (2003). HGF-, EGF-, and dexamethasone-induced gene expression patterns during formation of tissue in hepatic organoid cultures. *Gene Expr.* **11**, 55-75.

Miller, P. M., Folkmann, A. W., Maia, A. R., Efimova, N., Efimov, A. and Kaverina, I. (2009). Golgi-derived CLASP-dependent microtubules control Golgi organization and polarized trafficking in motile cells. *Nat. Cell Biol.* **11**, 1069-1080.

Oikawa, T., Kamiya, A., Kakinuma, S., Zeniya, M., Nishinakamura, R., Tajiri, H. and Nakauchi, H. (2009). Sall4 regulates cell fate decision in fetal hepatic stem/progenitor cells. *Gastroenterology* **136**, 1000-1011.

Ooshio, T., Fujita, N., Yamada, A., Sato, T., Kitagawa, Y., Okamoto, R., Nakata, S., Miki, A., Irie, K. and Takai, Y. (2007). Cooperative roles of Par-3 and afadin in the formation of adherens and tight junctions. *J. Cell Sci.* **120**, 2352-2365.

Parent, R. and Beretta, L. (2008). Translational control plays a prominent role in the hepatocytic differentiation of HepaRG liver progenitor cells. *Genome Biol.* **9**, R19.

Paris, L., Tonutti, L., Vannini, C. and Bazzoni, G. (2008). Structural organization of the tight junctions. *Biochim. Biophys. Acta* **1778**, 646-659.

Pollack, A. L., Apodaca, G. and Mostov, K. E. (2004). Hepatocyte growth factor induces MDCK cell morphogenesis without causing loss of tight junction functional integrity. *Am. J. Physiol. Cell Physiol.* **286**, C482-C494.

Puppo, F., Thomé, V., Lhoumeau, A. C., Cibois, M., Gangar, A., Lembo, F., Belotti, E., Marchetto, S., Lécine, P., Prébet, T. et al. (2011). Protein tyrosine kinase 7 has a conserved role in Wnt/β-catenin canonical signalling. *EMBO Rep.* **12**, 43-49.

Röttger, S., White, J., Wandall, H. H., Olivo, J. C., Stark, A., Bennett, E. P., Whitehouse, C., Berger, E. G., Clausen, H. and Nilsson, T. (1998). Localization of three human polypeptide GalNAc-transferases in HeLa cells suggests initiation of O-linked glycosylation throughout the Golgi apparatus. *J. Cell Sci.* **111**, 45-60.

Saulnier, N., Piscaglia, A. C., Puglisi, M. A., Barba, M., Arena, V., Pani, G., Alfieri, S. and Gasbarrini, A. (2010). Molecular mechanisms underlying human adipose tissue-derived stromal cells differentiation into a hepatocyte-like phenotype. *Dig. Liver Dis.* **42**, 895-901.

Schmelzer, E., Wauthier, E. and Reid, L. M. (2006). The phenotypes of pluripotent human hepatic progenitors. *Stem Cells* **24**, 1852-1858.

Synnergren, J., Heins, N., Brolén, G., Eriksson, G., Lindahl, A., Hyllner, J., Olsson, B., Sartipy, P. and Björquist, P. (2010). Transcriptional profiling of human embryonic stem cells differentiating to definitive and primitive endoderm and further toward the hepatic lineage. *Stem Cells Dev.* **19**, 961-978.

Szklarczyk, D., Franceschini, A., Kuhn, M., Simonovic, M., Roth, A., Minguez, P., Doerks, T., Stark, M., Muller, J., Bork, P. et al. (2011). The STRING database in 2011: functional interaction networks of proteins, globally integrated and scored. *Nucleic Acids Res.* **39**, D561-D568.

Takashi, H., Katsumi, M. and Toshihiro, A. (2007). Hepatocytes maintain their function on basement membrane formed by epithelial cells. *Biochem. Biophys. Res. Commun.* **359**, 151-156.

Turncliff, R. Z., Tian, X. and Brouwer, K. L. (2006). Effect of culture conditions on the expression and function of Bsep, Mrp2, and Mdr1a/b in sandwich-cultured rat hepatocytes. *Biochem. Pharmacol.* **71**, 1520-1529.

Wang, L. and Boyer, J. L. (2004). The maintenance and generation of membrane polarity in hepatocytes. *Hepatology* **39**, 892-899.

Wang, P., Zhang, H., Li, W., Zhao, Y. and An, W. (2008). Promoter-defined isolation and identification of hepatic progenitor cells from the human fetal liver. *Histochem. Cell Biol.* **130**, 375-385.

Yanai, H., Nakamura, K., Hijioka, S., Kamei, A., Ikari, T., Ishikawa, Y., Shinozaki, E., Mizunuma, N., Hatake, K. and Miyajima, A. (2010). Dlk-1, a cell surface antigen on foetal hepatic stem/progenitor cells, is expressed in hepatocellular, colon, pancreas and breast carcinomas at a high frequency. *J. Biochem.* **148**, 85-92.

Zamek-Gliszczynski, M. J., Xiong, H., Patel, N. J., Turncliff, R. Z., Pollack, G. M. and Brouwer, K. L. (2003). Pharmacokinetics of 5 (and 6)-carboxy-2′,7′-dichlorofluorescein and its diacetate promoiety in the liver. *J. Pharmacol. Exp. Ther.* **304**, 801-809.

Zhang, W., Li, W., Liu, B., Wang, P., Li, W. and Zhang, H. (2012). Efficient generation of functional hepatocyte-like cells from human fetal hepatic progenitor cells *in vitro*. *J. Cell. Physiol.* **227**, 2051-2058.

Zorn, A. M. (2008). Liver development. In *StemBook* (ed. The Stem Cell Research Community, StemBook). pp. doi/10.3824/stembook.1.25.1. http://www.stembook.org/node/512